Angular distributions in heavy-ion-induced fission

B. B. Back, R. R. Betts, J. E. Gindler, B. D. Wilkins, and S. Saini*
Chemistry Division, Argonne National Laboratory, Argonne, Illinois 60439

M. B. Tsang, C. K. Gelbke, and W. G. Lynch
National Superconducting Cyclotron Laboratory, Michigan State University, East Lansing, Michigan 48824

M. A. McMahan† and P. A. Baisden
Lawrence Livermore National Laboratory, Livermore, California 94558
(Received 24 January 1985)

Fission fragment angular distributions have been measured in reactions of $^{16}O+^{208}Pb$, ^{232}Th, ^{238}U, ^{248}Cm; $^{19}F+^{208}Pb$; $^{24}Mg+^{208}Pb$; $^{28}Si+^{208}Pb$; $^{32}S+^{197}Au$; and $^{32}S+^{208}Pb$ at several bombarding energies. The data are analyzed within the standard theory and it is found that the angular anisotropies for reactions with ^{24}Mg and heavier projectiles are significantly larger than expected theoretically. Comparative studies of reactions in which different target-projectile combinations are leading to similar fissioning systems show that the large angular anisotropies are associated with the charge (and mass) of the projectile. This excludes large angular momenta and temperatures as the cause of these discrepancies. It is concluded that the onset of the quasifission reaction is responsible for the large observed anisotropies.

I. INTRODUCTION

The standard theory of fission angular distributions is based on the assumption[1] that the fission fragments are emitted in the direction of the nuclear symmetry axis at the fission saddle point. The orientation of the symmetry axis is expressed in terms of the component K of the total spin vector $\bar{I}$ onto the symmetry axis, the underlying physical assumption being that the Coriolis forces acting on the system as it elongates from saddle to scission are of insufficient strength to significantly alter the K value selected by the system during the passage over the saddle. Provided that this assumption is valid, a measurement of the angular distribution of final fragments will provide information on the K value of the system during passage over the saddle point if the spin (I and M) of the fissioning nucleus is known. In the statistical regime, it has been shown[2] that there is a simple relation between the nuclear temperature, the nuclear shape, and the distribution of K values at the saddle point. Under these conditions, fission fragment angular distributions can provide unique information about the nuclear saddle point shape which can be directly compared to theoretical predictions. Fission of compound nuclei formed in fusion reactions is well suited for this purpose since the average nuclear spin and its projection, M, is well under control in such reactions. The results of a study of such reactions,[3,4] namely 42.8 MeV α particles on a range of targets from ^{230}Th to ^{249}Cf, are shown in Fig. 1. The measured saddle point deformation (expressed in terms of the moments of inertia) is compared to the prediction of the liquid drop model[5] as a function of the fissility parameter x, which expresses the stability of the nucleus against fission. From this comparison we observe that the experimental data reflect both the magnitude and the x dependence of the saddle point deformation. There is no indication that the Coriolis forces are strong enough to change the K distribution toward achieving a statistical equilibrium at the scission point, the shape of which is also indicated in Fig. 1 in terms of its moments of inertia. From the outset, it was not obvious that the K distribution, established at the saddle point, would be preserved during the motion toward scission, but these, and a large body of experimental data, strongly support this assumption.

With the availability of energetic heavy ion beams, there has recently been a renewed interest in the measurement of the angular distributions of fission fragments from heavier systems[6–16] with high angular momenta. The fission decay of compound nuclei formed in heavy ion fusion reactions is expected to provide a more stringent test of the standard theory because of the increased strength of the Coriolis forces at the high angular velocities reached in such reactions. Also the possibility of producing systems with no stability against fission[17] presents an interesting challenge for testing the standard concepts.

In the present study we have measured the fission fragment angular distributions from the reactions $^{16}O+^{208}Pb$, ^{232}Th, ^{238}U, ^{248}Cm; ^{19}F, ^{24}Mg, $^{28}Si+^{208}Pb$; and $^{32}S+^{197}Au$, ^{208}Pb at several beam energies above the interaction barrier. These data, and most heavy ion induced fission data appearing in the literature are submitted to a careful analysis based on the standard theory with emphasis on realistic estimates of the spin distribution of the fissioning systems. This analysis shows that the standard theory is valid, even for quite heavy nuclei fissioning with high angular momentum, provided that compound nucleus formation is achieved in the reaction. Nevertheless, if the fission barrier becomes smaller than the nuclear temperature, due to a combination of high excitation ener-

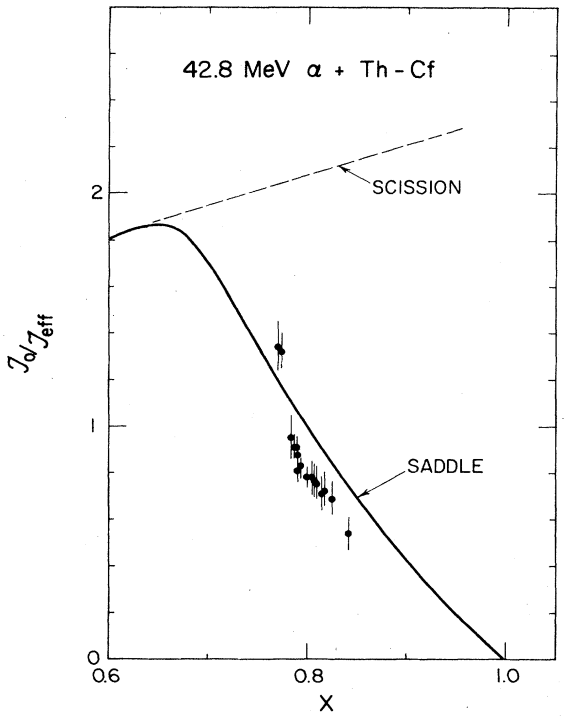

FIG. 1. Effective moments of inertia $\mathcal{J}_0/\mathcal{J}_{\text{eff}}$ resulting from the analysis of angular distributions for 42.8 MeV α-induced fission on a range of targets from ^{232}Th—^{249}Cf, Ref. 4, are plotted as a function of the fissility parameter and compared with the saddle point shapes (solid curve) predicted by the liquid drop model.[5] The $\mathcal{J}_0/\mathcal{J}_{\text{eff}}$ values associated with the expected scission shapes are also shown (dashed curve).

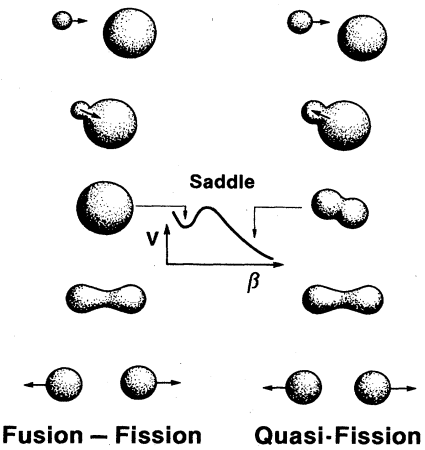

FIG. 2. Schematic illustration of the difference between fusion-fission (left) and quasifission reactions (right). Only fusion-fission reactions carry information about the shape of the saddle point, because it is traversed during the fission decay, whereas the quasifission, by definition, does not reach shapes inside the fission barrier.

gy and charge or angular momentum of the fissioning system, we do observe deviations from the theory.

Much larger deviations are observed in comparative studies in which two systems with the same fissility x are produced through different projectile-target combinations. If both reactions proceed through the stage of compound nucleus formation, one should expect identical saddle point shapes, and the angular distributions should be independent of the target-projectile combination. But the analysis of such data indicates substantially larger saddle deformations in reactions involving heavy projectiles (^{28}Si and ^{32}S) than those involving lighter projectiles (^{16}O, ^{19}F). This result is found irrespective of the spin of the fissioning system, which leads to the conclusion that the large deformations seen for heavy projectiles arise from an inability to form genuine compound systems inside the fission saddle point. Although the fission fragments from these reactions have kinetic energies and mass distributions typical for the fission of compound nuclei, we conclude that the shape of the intermediate system, at which the K distribution is determined, depends on the mass asymmetry of the *entrance* channel, as illustrated in Fig. 2.

The reactions with heavy projectiles show properties which are typical of the quasifission reaction mechanism. This reaction channel is generally characterized by full energy relaxation and a substantial mass drift toward symmetry without compound nucleus formation. In the cases studied in the present work, the mass drift toward symmetry is essentially completed before reseparation occurs. In heavier systems,[18,19] the reaction time is shorter ($\tau < 10^{-20}$ s), and the mass equilibration is only partially completed when reseparation occurs. In general, we therefore observe a gradual change in character of the quasifission reaction with heavy targets as a function of projectile mass. For rather light projectiles, $A \sim 30$, the mass drift toward symmetry is complete, and the occurrence of quasifission can only be discerned on the basis of a detailed quantitative analysis of the fragment angular distributions as discussed in this work, the hallmark being that the fission direction remains more closely perpendicular to the direction of the angular momentum than expected for true compound nucleus fission. With increasing projectile mass the reaction times become shorter, and distinct fragment mass-scattering angle correlations are observed, revealing the direct character of the reaction mechanism.

The present article is organized in the following way. The experimental procedure is presented in Sec. II. This is followed by a presentation of the standard theory for fission angular distributions along with a brief discussion of the validity of basic assumptions of the theory in Sec. III. The experimental angular distributions are presented and analyzed in Sec. IV and a discussion of the total fission cross sections is given in Sec. V. Finally, Sec. VI summarizes the results.

II. EXPERIMENTAL PROCEDURE

Beams of ^{16}O, ^{19}F, ^{24}Mg, ^{28}Si, and ^{32}S obtained from the Argonne Superconducting Linac were focused onto targets of thickness 100–250 μg/cm^2 located in the center of a 45 cm diam scattering chamber. Single fission fragments were detected in the angular range $\theta = 10°$–$174°$ by using one or two Si-detector telescopes, consisting of a

5–9 μm thick ΔE detector with an area of 50 mm^2 backed by a 100 mm^2, 60 μm thick fission detector, see Fig. 3. Fission fragments emitted in backward angles were measured in 2–3 100 mm^2, 60 μm thick fission detectors. The detectors were located 17–18 cm from the target allowing for an approximate time-of-flight determination of the fragment masses by making use of a fast timing pulse from the detectors and the radio frequency of the linac, which resulted in a time resolution of 200–300 ps FWHM. This time resolution is sufficient to isolate fission fragments from other reaction products in all detectors. On the other hand, the mass- and energy-dependent plasma delay[20] of the time signals from the Si detectors, which can amount to $\sim$500 ps, combined with the short flight paths did not allow us to obtain precise information on the mass distributions by this method. Two monitor detectors, mounted at $\pm 15°$ relative to the beam axis, were used for normalization purposes. In the transformation from the laboratory to the center-of-mass frame of reference we have used the kinematics relevant for symmetric fission with kinetic energies taken from the Viola systematics.[21] This procedure is justified by the forward-backward symmetry observed in the resulting center-of-mass angular distribution and by the theoretical analysis of this problem performed by Ho and Gonthier.[22]

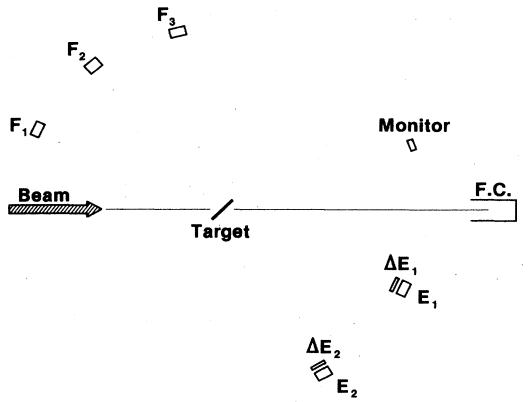

FIG. 3. Schematic illustration of the experimental arrangement.

III. ANGULAR DISTRIBUTIONS—THEORY

In the standard theory of fission angular distributions it is assumed that the final direction of fragments is given by the orientation of the nuclear symmetry axis as the nucleus passes over the fission saddle point.[1] It is here implicitly assumed that the nucleus is formed initially in a configuration inside the fission barrier, an assumption which may not be fulfilled, when heavy projectiles are used, as will be demonstrated later. It is also normally argued that the Coriolis force and other effects violating K conservation are of insufficient strength to alter the K value during the rapid descent from saddle to scission (K is the projection of the total spin I onto the nuclear symmetry axis). This assumption may not be justified for the heaviest systems studied in the present work, for which the saddle and scission point configurations have very different shapes.

Under the standard assumptions, the angular distribution of fission fragments is given by the symmetric top wave functions as follows:

$$W^I_{MK}(\theta)=\frac{2I+1}{4\pi}\,|\,\mathscr{D}^I_{MK}(\phi,\theta,\psi)\,|^2\,. \tag{1}$$

This expression reduces to

$$W^I_{0K}(\theta)=\frac{2I+1}{4\pi}\,|\,d^I_{0K}(\theta)\,|^2 \tag{2}$$

for fusion of spin zero nuclei for which spin projection, M, onto the beam axis is zero, and the two other Euler angles ψ and ϕ disappear by taking the absolute square, such that only the dependence on the angle θ between the beam axis and the nuclear symmetry axis remains in the expression.

In order to compare with experimental data, it is necessary to average over the spin I and the K quantum number. Using arguments based on the statistical model with a constant temperature level density, Halpern and Strutinski[2] have derived the following expression for the K distribution

$$\rho(K)=\frac{\exp(-K^2/2K_0^2)}{\sum_{K=-I}^{I}\exp(-K^2/2K_0^2)};\quad K\le I\,,$$
$$=0;\quad K>I\,, \tag{3}$$

where

$$K_0^2=\frac{\mathscr{I}_{\rm eff}}{\hbar^2}T;\quad \mathscr{I}_{\rm eff}^{-1}=\mathscr{I}_{\parallel}^{-1}-\mathscr{I}_{\perp}^{-1}\,. \tag{4}$$

The distribution of K values is therefore Gaussian with a standard deviation K_0, which is related to the nuclear temperature, T, and the moments of inertia, $\mathscr{I}_{\parallel}$ and $\mathscr{I}_{\perp}$, for rotations around the symmetry axis and a perpendicular axis, respectively. The nuclear temperature at the saddle point, T, is given by the expression $T^2=8.5(E^*-B_f-E_{\rm rot})/A$, where E^* is the excitation energy of the compound nucleus, B_f is the fission barrier, and $E_{\rm rot}$ is the rotational energy. We thus arrive at the following expression for the fragment angular distribution,

$$W(\theta)=\sum_{I=0}^{\infty}(2I+1)T_I\frac{\sum_{K=-I}^{I}\frac{1}{2}(2I+1)d^I_{0K}(\theta)^2\exp[-K^2/2K_0^2(I)]}{\sum_{K=-I}^{I}\exp[-K^2/2K_0^2(I)]}\,. \tag{5}$$

In this expression, T_l is the transmission coefficient for fusion of the lth partial wave and $K_0(I)$ is the standard deviation of the K distribution for spin I states. Direct numerical calculations of the d function for large I values are complicated by the fact that it is given by an alternating sum of almost canceling terms. This difficulty is circumvented by the use of certain recursion relations, as described in Appendix A. In Appendix A, we also give a comparison with the often used classical approximation for the fission angular distributions.

A. Spin distributions in fusion reactions

Classical models for fusion between spherical heavy ions result in triangular spin distributions corresponding to an abrupt change in the fusion probability at that partial wave for which the radial center-of-mass energy matches the fusion barrier. It is evident that triangular spin distributions are very unrealistic at near-barrier energies, where the effects of tunneling and barrier fluctuations introduce tails of the spin distributions which are comparable to or larger than the maximum spin value of the classical sharp cutoff model. Since the experimental fission anisotropy is a measure of the ratio $K_0/\langle I\rangle$, where $\langle I\rangle$ is the average spin of the fissioning system, it is of central importance to obtain realistic estimates of $\langle I\rangle$ and the associated uncertainties. We have attempted to do this by (1) using the proximity description for the nuclear interaction to estimate the fusion barrier height and (2) using the barrier fluctuations arising from both static[23–25] and dynamic[26,27] fluctuations of the distance of the nuclear surface from the center of mass. Details of the calculation of the partial wave fusion probabilities are discussed in Appendix B.

B. Spin dependent saddle point shapes

In the analysis of fission angular distributions from low spin states it is normally assumed that the moments of inertia at the saddle point are constant over the range of spins in question, i.e., $K_0(I)=K_0=\text{const}$. Such data are therefore analyzed by varying the value of K_0^2 until a satisfactory fit to the data is obtained. The corresponding value of the parameter $\mathcal{I}_0/\mathcal{I}_{\text{eff}}$, where $\mathcal{I}_0$ is the rigid moment of a sphere of equal volume, can then be directly compared with theoretical estimates of the liquid drop model.[5]

In heavy-ion-induced fission, however, one often deals with a large range of angular momenta for which the assumption of a spin independent saddle point shape is not justified. The rotating liquid drop model[17] predicts that the saddle point deformation of heavy nuclei ($x \geq 0.7$) depends critically not only on the nuclear charge, but also on the amount of angular momentum perpendicular to the symmetry axis. When heavy-ion-induced fission angular distributions are analyzed in this manner, one must therefore expect that the resulting values of $\mathcal{I}_0/\mathcal{I}_{\text{eff}}$ will depend on the average angular momentum of the fissioning system, which increases with beam energy. For a detailed discussion of our analysis of the data see Sec. IV.

C. Assumption of K conservation

The main empirical evidence for the assumption of unchanged K values during the descent from saddle to scission is summarized in Fig. 1, and discussed in the Introduction, Sec. I. It has been pointed out,[6,28] however, that this assumption must break down in the limit of very heavy compound nuclei with high spins, if such nuclei can be produced. Since the spins of the fission fragments are limited by the yrast line, fission decay with the largest K values allowed at the saddle may be inhibited because of angular momentum conservation.[29] Exactly when this breakdown of K conservation sets in, is presently unknown from experimental studies because of experimental difficulties in ensuring that a compound nucleus has been formed in a fusion-fission reaction. It is thus difficult to verify whether observed deviations from the rotating liquid drop model[17] estimates arise from changes in the K distribution during the descent from saddle to scission or by a failure to produce a compound nucleus. In the latter case, K distributions are expected to be narrower than those estimated at saddle point shapes. We therefore rely on comparisons between different entrance channels reaching similar compound systems in order to shed light on this question.

If a compound nucleus is formed in the reaction, different target projectile combinations leading to nearly identical compound systems must necessarily show very similar angular distributions. Models[29,30] which are based on the assumption that the K distribution is determined at the scission point are therefore incapable of explaining the observed entrance channel dependence of the fission anisotropies. Entrance channel effects are a clear indication of a more direct reaction mechanism.

In Sec. IV we will present evidence for such entrance channel effects.

D. Post scission K breaking

Changes in the K value which occur after scission also come into play when the angular momenta are large. Since the motion after scission is governed simply by long-range Coulomb forces, the change can be estimated in a classical calculation of the post-scission trajectories as detailed in Appendix C. The following approximate expression is obtained

$$K_0 = K_0^f(1+2E_{\text{rot}}/V_{\text{Coul}}) , \tag{6}$$

where K_0^f and K_0 are the standard deviations of the final K distribution and the uncorrected K distribution, respectively. The quantities E_{rot} and V_{Coul} are the centrifugal energy and the Coulomb potential at scission, respectively, which are estimated in the touching equal spheres approximation (see Appendix C). In some cases this correction amounts to 10% and is therefore applied in the analysis discussed in Sec. IV.

E. K-dependent saddle point shapes

It has recently been suggested[31] that the assumption of K independence of the saddle point shapes may not be valid in heavy-ion-induced fission. The rotating liquid

drop model[17] is concerned strictly with $K=0$ states only and cannot elucidate this problem, although a generalization to $K\neq 0$ states is presently being investigated.[31] Intuitively one would expect that such corrections will come into play only for the very heaviest systems where the ratio $K_0^2/\langle I^2\rangle$ approaches unity because of the contraction of the fission saddle point towards sphericity. For the systems studied in the present work we find $K_0^2 \ll \langle I^2\rangle$ except possibly for the $^{16}O+^{248}Cm$ system. We therefore expect this effect to be of minor importance in our analysis. Although forthcoming theoretical calculations[31] undoubtedly will shed more light on this problem, we have chosen to disregard it here since it appears that the observed deviations from the standard theory are related more directly to the entrance channel mass asymmetry.

IV. EXPERIMENTAL ANGULAR DISTRIBUTIONS

The single fragment angular distributions measured in the present work are shown as solid points in Figs. 4–7. The solid curves represent the best fits to the data using a least squares fitting procedure in connection with Eq. (5). Measured fission cross sections and the extracted angular anisotropies for the various reactions are listed in Table I. The values of the parameter $\mathcal{J}_0/\mathcal{J}_{\text{eff}}$ extracted from the analysis with one K_0^2 value for each beam energy are plotted as a function of the mean square spin $\langle I^2\rangle$ of the fissioning system in Fig. 8 and listed in Table II along with parameters relevant to the analysis. The present values of the $\mathcal{J}_0/\mathcal{J}_{\text{eff}}$ parameter are somewhat smaller than the results of an earlier analysis[10,11] of the same data. This discrepancy arises from the choice of a smaller radius parameter, $r_0=1.16$ fm, as compared with the previously

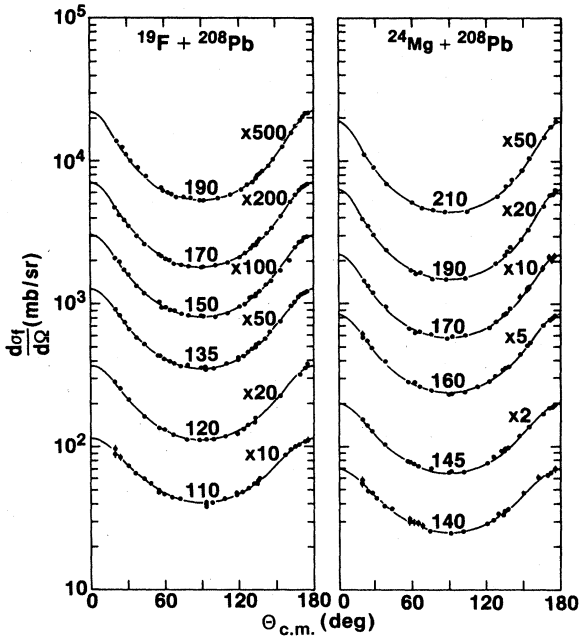

FIG. 5. Experimental angular distributions of fission fragments from the reactions ^{19}F, $^{24}Mg+^{208}Pb$. Each set of data is labeled with the beam energy in MeV. Error bars indicate statistical errors.

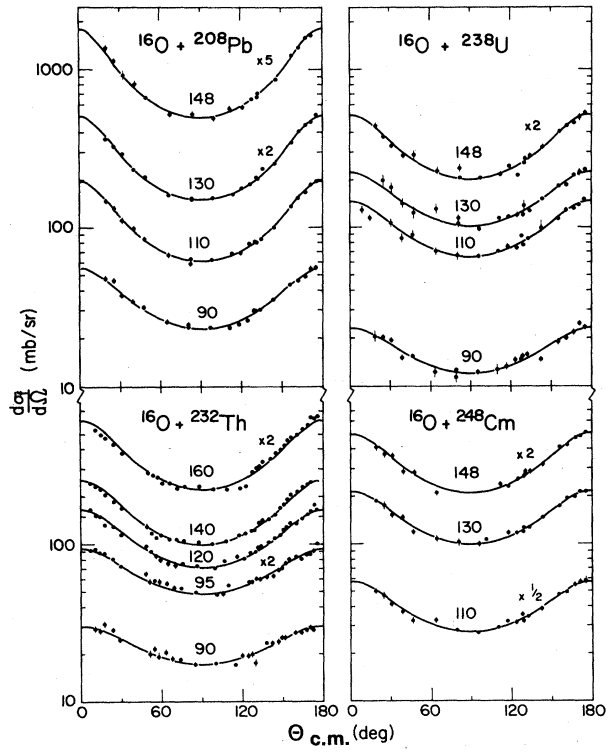

FIG. 4. Experimental angular distributions of fission fragments from the reactions $^{16}O+^{208}Pb$, ^{232}Th, ^{238}U, ^{248}Cm. Each set of data is labeled with the beam energy in MeV. Error bars indicate statistical errors.

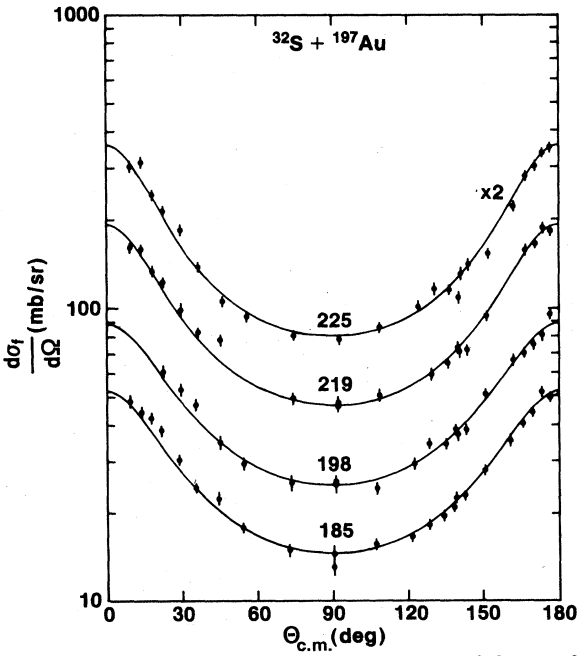

FIG. 6. Experimental angular distributions of fission fragments from the reaction $^{32}S+^{197}Au$. Each set of data is labeled with the beam energy in MeV. Error bars indicate statistical errors.

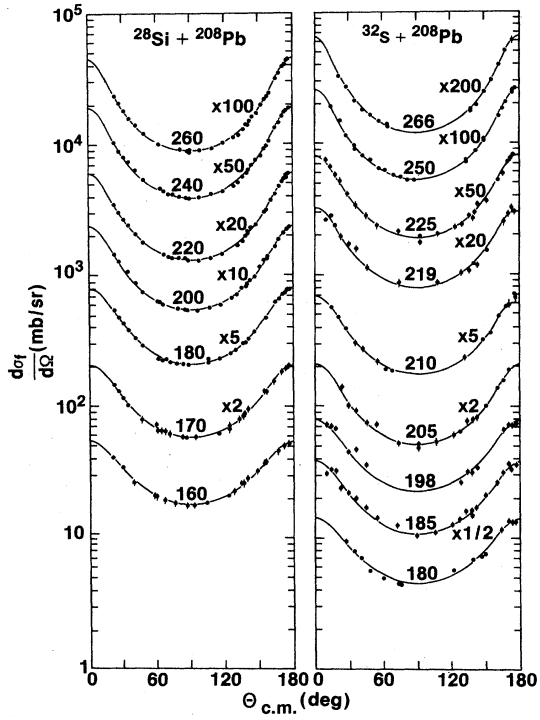

FIG. 7. Experimental angular distributions of fission fragments from the reactions ^{28}Si, ^{32}S + ^{208}Pb. Each set of data is labeled with the beam energy in MeV. Error bars indicate statistical errors.

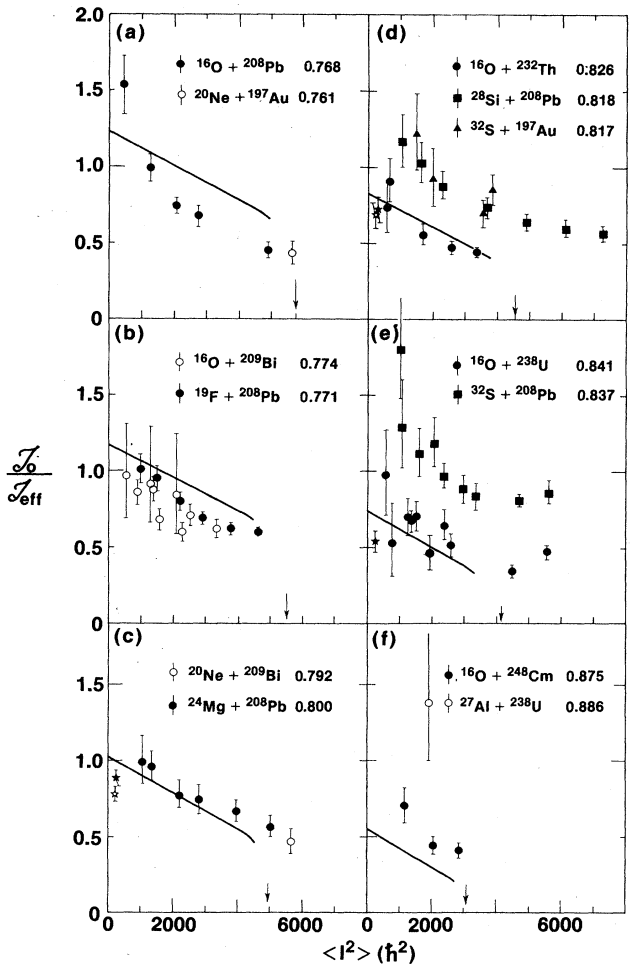

FIG. 8. Experimental $\mathcal{J}_0/\mathcal{J}_{eff}$ values (points) are plotted as a function of the mean square spin $\langle I^2 \rangle$ of the fissioning system. Reactions associated with the same values of the fissility x of the combined system are compared. Solid curves represent the predictions of the rotating liquid drop model (Ref. 17). The arrow points to the angular momenta at which the fission barrier is predicted to vanish. Stars correspond to α-induced reactions (Ref. 4).

used value of $r_0 = 1.225$ fm in the estimate of the rigid moments of inertia. A justification for this choice is given in Sec. V. Since the saddle point shape (and consequently $\mathcal{J}_0/\mathcal{J}_{eff}$), and the fission barrier height of a nucleus depend only on the fissility x of the fissioning system, we have ordered the data such that reactions leading to composite systems with approximately the same fissility x are compared. In the liquid drop model, the fissility is defined as

$$x = \frac{Z^2/A}{50.883\{1 - 1.7826[(N-Z)/A]^2\}} , \quad (7)$$

where Z, N, and A are the proton, neutron, and mass number, respectively. Aside from the data obtained in the present work, we have also analyzed some relevant published data.[4,12–16] The solid lines in Fig. 8 represent the predicted spin dependence of $\mathcal{J}_0/\mathcal{J}_{eff}$ of the rotating liquid drop model (RLDM).[17] The arrows indicate where the fission barrier vanishes.

It is observed that saddle point shapes derived from reactions with α, ^{16}O, ^{19}F, ^{20}Ne, and ^{24}Mg beams are in reasonable agreement with the RLDM predictions, although there is a tendency to obtain lower $\mathcal{J}_0/\mathcal{J}_{eff}$ values than predicted for the lighter systems. The expected angular momentum dependence corresponding to more compact saddle point shapes at higher spins is well reproduced by the data. There is little direct evidence for the readjustment of the K distribution during the descent from saddle to scission. Such a readjustment might manifest itself as a leveling out of the $\mathcal{J}_0/\mathcal{J}_{eff}$ values for sufficiently large spins since the high K values would be suppressed by the inability of the fission fragments to support high spin values.[29] For the ^{16}O + ^{248}Cm system, the observed deviation from the RLDM prediction is probably related to the small fission barrier of less than 1 MeV. At such small values, the fission barrier loses its significance in determining the fission anisotropies.[12]

A further complication, of experimental nature, is expected in reactions with ^{232}Th, ^{238}U, and, in particular, ^{248}Cm targets, because the present experiment cannot distinguish fission following complete fusion from sequential fission after quasielastic or deeply inelastic reactions. Contamination from sequential fission following such reactions should, however, lead to reduced anisotropies, i.e., reduced $\mathcal{J}_0/\mathcal{J}_{eff}$ values. As discussed in more detail in Appendix D, it seems unlikely that this type of contamination is responsible for the observed discrepancy in the ^{16}O + ^{248}Cm system.

TABLE I. Experimental fission cross sections and anisotropies.

Reaction	Compound nucleus	x	E_{lab} (MeV)	$\sigma_{fission}$ (mb)	$\frac{W(0°)}{W(90°)}$
$^{16}O+^{208}Pb$	^{224}Th	0.763	90	370±20	2.42
			110	1060±50	3.13
			130	1315±65	3.36
			148	1770±90	3.58
$^{16}O+^{232}Th$	^{248}Cf	0.826	90	255±15	1.75
			95	370±20	1.93
			120	1150±60	2.32
			140	1655±85	2.54
			160	1880±95	2.71
$^{16}O+^{238}U$	^{254}Fm	0.842	90	185±10	1.92
			110	1040±55	2.24
			130	1620±80	2.20
			148	1670±100	2.55
$^{16}O+^{248}Cm$	$^{264}_{104}X$	0.875	110	850±45	2.11
			130	1565±80	2.16
			148	1700±85	2.38
$^{19}F+^{208}Pb$	^{227}Pa	0.771	110	685±35	2.79
			120	965±50	3.29
			135	1245±65	3.58
			150	1440±75	3.75
			170	1615±80	3.92
			190	1910±95	4.16
$^{24}Mg+^{208}Pb$	^{232}Pu	0.800	140	420±25	2.78
			145	555±30	3.08
			160	835±45	3.53
			170	1025±50	3.84
			190	1345±70	4.22
			210	1584±80	4.28
$^{28}Si+^{208}Pb$	^{236}Cm	0.818	160	305±15	3.01
			170	510±25	3.49
			180	740±40	3.84
			200	990±50	4.31
			220	1185±60	4.57
			240	1430±75	4.84
			260	1630±85	5.04
$^{32}S+^{197}Au$	^{229}Am	0.817	185	250±15	3.60
			198	435±25	3.56
			219	830±45	4.12
			225	725±40	4.45
$^{32}S+^{208}Pb$	^{240}Cf	0.837	180	155±20	3.12
			185	190±20	3.53
			198	390±25	3.49
			205	460±25	4.05
			210	615±35	3.89
			219	710±40	4.11
			225	685±40	4.24
			250	975±50	4.86
			266	1115±60	5.40

For the reactions shown in sections (a), (b), and (c) of Fig. 8, projectiles with mass ≤ 24 are used. We observe that the extracted $\mathcal{J}_0/\mathcal{J}_{eff}$ values depend mainly on the fissility x of the fissioning system. They are, on the other hand, quite insensitive to variations in the projectile-target combination. This picture changes when going to reactions involving ^{27}Al, ^{28}Si, and ^{32}S projectiles, as displayed in Figs. 8(d), (c), and (f). In these cases, we find a strong entrance channel dependence on the $\mathcal{J}_0/\mathcal{J}_{eff}$ values for systems with similar fissilities. This discrepancy is not just an effect of larger angular momenta being brought into the system by the heavy projectiles, since it exists also for moderate spins. Furthermore, the α-particle and ^{16}O-induced reactions are in good agreement. The large fission fragment anisotropies, which are generally observed in fission reactions with heavy projectiles, $A \geq 25$–27, are

TABLE II. Parameters relevant for the analysis of the fission angular distribution data.

Reaction	Compound nucleus	x	E_{lab} (MeV)	σ[a] (mb)	$\langle I^2 \rangle$ ($\hbar^2$)	$\frac{W(0°)}{W(90°)}$	T_{saddle}[b] (MeV)	K_0[b] ($\hbar$)	$\mathcal{J}_0/\mathcal{J}_{eff}$ uncorrected	$\mathcal{J}_0/\mathcal{J}_{eff}$ corrected[c]	$\mathcal{J}_0/\mathcal{J}_{eff}$ RLDM[b]	Ref.
$^{16}O+^{208}Pb$	^{224}Th	0.763	90	390	435	2.42	1.14	8.8	1.54±0.20	1.53±0.20	1.18	This work
			110	1060	1275	3.13	1.37	11.9	1.01±0.10	0.99±0.09	1.10	This work
			130	1485	2085	3.36	1.56	14.6	0.77∓0.05	0.74±0.05	1.00	This work
			148	1740	2780	3.58	1.72	15.9	0.71±0.06	0.67±0.07	0.92	This work
			215	2115	4935	3.53	2.21	21.6	0.50±0.06	0.45±0.05	0.68	9
$^{16}O+^{209}Bi$	^{225}Pa	0.774	94	490	540	2.11	1.17	11.3	0.98±0.30	0.97±0.30	1.11	14
			102	770	870	2.48	1.27	12.4	0.88±0.10	0.86±0.10	1.07	13
			112	1055	1290	3.05	1.38	12.5	0.94±0.26	0.91±0.25	1.03	14
			117	1075	1370	3.03	1.44	12.9	0.91±0.10	0.88±0.10	1.01	13
			119	1225	1580	2.85	1.44	14.7	0.71±0.10	0.68±0.10	0.99	13
			134	1500	2175	3.64	1.59	13.9	0.88±0.26	0.84±0.25	0.92	14
			137	1545	2285	3.11	1.61	16.4	0.64±0.10	0.60±0.10	0.91	13
			143	1635	2525	3.54	1.67	15.3	0.75±0.10	0.71±0.10	0.88	13
			166	1865	3350	3.64	1.85	17.1	0.66±0.10	0.62±0.10	0.78	13
$^{16}O+^{232}Th$	^{248}Cf	0.826	90	250	595	1.75	1.23	14.5	0.74±0.16	0.73±0.16	0.76	This work
			95	390	640	1.93	1.29	13.3	0.92±0.14	0.91±0.14	0.75	This work
			120	1150	1695	2.32	1.52	18.3	0.57±0.07	0.55±0.07	0.63	This work
			140	1610	2575	2.54	1.69	20.8	0.49±0.05	0.47±0.04	0.53	This work
			160	1850	3335	2.71	1.84	22.3	0.46±0.04	0.44±0.04	0.45	This work
$^{16}O+^{238}U$	^{254}Fm	0.842	90	185	560	1.92	1.19	12.6	0.98±0.26	0.97±0.26	0.67	This work
			96	360	745	1.62	1.26	17.7	0.52±0.21	0.52±0.21	0.65	16
			110	855	1255	2.24	1.40	16.1	0.71±0.12	0.69±0.12	0.59	This work
			114	965	1465	2.46	1.41	16.0	0.72±0.10	0.70±0.10	0.56	14
			114	965	1465	2.25	1.41	16.4	0.69±0.07	0.67±0.07	0.56	12
			130	1250	1980	2.20	1.58	20.8	0.48±0.12	0.46±0.12	0.49	This work
			140	1410	2375	2.81	1.66	18.1	0.67±0.10	0.64±0.10	0.45	12
			148	1450	2575	2.55	1.73	20.6	0.53±0.07	0.51±0.07	0.42	This work
			215	1750	4475	2.47	2.19	28.2	0.36±0.04	0.34±0.04	0.19	9
			250	1870	5555	3.18	2.41	24.9	0.51±0.05	0.47±0.05		12
$^{16}O+^{248}Cm$	$^{264}_{104}X$	0.875	110	745	1145	2.11	1.34	16.3	0.71±0.12	0.70±0.12	0.41	This work
			130	1280	2065	2.16	1.51	21.6	0.45±0.06	0.44±0.06	0.29	This work
			148	1610	2865	2.38	1.65	23.3	0.43±0.06	0.41±0.06	0.19	This work
$^{19}F+^{208}Pb$	^{227}Pa	0.771	110	680	970	2.79	1.31	11.7	1.03±0.10	1.01±0.10	1.10	This work
			120	970	1470	3.29	1.41	12.4	0.98±0.09	0.95±0.09	1.03	This work
			135	1250	2195	3.58	1.54	14.1	0.83±0.07	0.80±0.07	0.95	This work
			150	1550	2900	3.75	1.67	15.6	0.74±0.05	0.69±0.04	0.88	This work
			170	1785	3780	3.92	1.82	17.1	0.67±0.04	0.62±0.04	0.79	This work
			190	1950	4615	4.12	1.97	17.9	0.66±0.03	0.60±0.03	0.71	This work
$^{20}Ni+^{197}Au$	^{217}Ac	0.761	220	1920	5575	3.86	2.21	21.1	0.49±0.08	0.43±0.08		15
$^{20}Ne+^{209}Bi$	^{229}Np	0.792	220	1970	5635	3.94	2.07	20.9	0.52±0.08	0.47±0.08	0.38	15

TABLE II. (*Continued*).

Reaction	Compound nucleus	x	E_{lab} (MeV)	σ[a] (mb)	$\langle I^2 \rangle$ ($\hbar^2$)	$\frac{W(0°)}{W(90°)}$	T_{saddle}[b] (MeV)	K_0[b] ($\hbar$)	$\mathcal{J}_0/\mathcal{J}_{eff}$ uncorrected	$\mathcal{J}_0/\mathcal{J}_{eff}$ corrected[c]	$\mathcal{J}_0/\mathcal{J}_{eff}$ RLDM[b]	Ref.
$^{24}Mg+^{208}Pb$	^{232}Pu	0.800	140	440	1035	2.78	1.30	12.0	1.01±0.16	0.99±0.16	0.88	This work
			145	565	1315	3.08	1.35	12.4	0.98±0.10	0.96±0.10	0.85	This work
			160	900	2210	3.53	1.48	14.3	0.81±0.10	0.77±0.10	0.75	This work
			170	1080	2790	3.84	1.56	14.9	0.78±0.10	0.74±0.10	0.68	This work
			190	1370	3930	4.22	1.71	16.3	0.71±0.08	0.66±0.08	0.54	This work
			210	1580	5000	4.28	1.84	18.2	0.62±0.08	0.56±0.08	0.42	This work
$^{27}Al+^{238}U$	$^{265}_{105}X$	0.886	162	400	1895	3.84	1.36	11.7	1.40±0.40	1.37±0.40	0.22	16
$^{28}Si+^{208}Pb$	^{236}Cm	0.818	160	310	1045	3.01	1.27	11.1	1.18±0.16	1.16±0.16	0.76	This work
			170	520	1620	3.49	1.37	12.3	1.05±0.13	1.02±0.13	0.68	This work
			180	730	2305	3.84	1.44	13.5	0.91±0.09	0.87±0.09	0.60	This work
			200	1060	3635	4.31	1.59	15.4	0.77±0.07	0.73±0.07	0.43	This work
			220	1200	4910	4.57	1.72	17.0	0.69±0.06	0.63±0.06	0.27	This work
			240	1430	6100	4.84	1.85	18.0	0.66±0.06	0.59±0.06	0.11	This work
			260	1630	7260	5.04	1.98	19.0	0.63±0.05	0.56±0.05		This work
$^{32}S+^{197}Au$	^{229}Am	0.817	185	250	1480	3.60	1.41	11.1	1.25±0.25	1.21±0.25	0.69	This work
			198	425	1990	3.56	1.51	13.2	0.95±0.20	0.92±0.20	0.62	This work
			219	830	3540	4.12	1.65	15.7	0.73±0.09	0.69±0.09	0.42	This work
			225	850	3825	4.45	1.70	15.2	0.80±0.10	0.75±0.10	0.38	This work
$^{32}S+^{208}Pb$	^{240}Cf	0.837	180	150	1055	3.12	1.27	10.7	1.31±0.30	1.29±0.30	0.62	This work
			185	190	1005	3.53	1.34	9.4	1.82±0.32	1.79±0.32	0.62	This work
			198	390	1625	3.49	1.45	12.2	1.14±0.15	1.11±0.15	0.55	This work
			205	500	2060	4.05	1.51	12.1	1.22±0.15	1.18±0.15	0.50	This work
			210	570	2360	3.89	1.54	13.5	1.01±0.08	0.97±0.08	0.46	This work
			219	690	2930	4.11	1.60	14.3	0.92±0.09	0.88±0.09	0.39	This work
			225	770	3330	4.24	1.64	14.9	0.88±0.08	0.83±0.08	0.33	This work
			250	990	4710	4.86	1.81	15.7	0.87±0.05	0.81±0.05	0.17	This work
			266	1110	5605	5.40	1.92	15.6	0.94±0.07	0.86±0.07		This work
$^{32}S+^{232}Th$	$^{264}_{106}X$	0.899	218	815	3935	2.88	1.51	22.7	0.41±0.07	0.39±0.07		6
$^{32}S+^{238}U$	$^{270}_{108}X$	0.914	218	770	4075	2.45	1.48	26.9	0.30±0.10	0.29±0.10		6
$^{32}S+^{248}Cm$	$^{280}_{112}X$	0.948	218	670	3990	2.75	1.42	23.6	0.39±0.10	0.38±0.10		6
$^{40}Ar+^{238}U$	$^{278}_{110}X$	0.927	340	1140	8985	6.48	2.02	16.6	1.12±0.60	1.01±0.60		7

[a]Total cross section for fission following full momentum transfer reactions, i.e., excluding sequential fission. These numbers represent best estimates based on either cross section calculations, (see Sec. V), or smooth interpolations of experimental data.

[b]Estimated at the mean square spin of fissioning nuclei.

[c]Corrected for post-scission reorientation, see Appendix C.

not exclusively related to the properties of the compound systems. On the contrary, it is seen to depend mainly on the entrance channel asymmetry. The fission fragments observed in the $^{28}Si+^{208}Pb$, $^{32}S+^{197}Au$, $^{32}S+^{208}Pb$, and $^{27}Al+^{238}U$ cannot arise from normal fission decay of truly equilibrated compound nuclei, which, by definition, do not keep memory of the entrance channel (except for conserved quantities, Z, A, I, etc.). Reactions which do not proceed through the formation of a compound nucleus are likely to involve a different sequence of intermediate states in which mass and energy equilibration is achieved. This view of the reactions places them in a category with the reactions of heavier projectiles[18,19] where incomplete mass relaxation clearly takes place via a nonequilibrium (direct) mechanism.

In an attempt to display the tendency to deviate from the predicted saddle point shapes in a systematic way we have extended the present analysis to essentially all available data on heavy-ion-induced fission leading to composite systems heavier than ^{224}Th. Also the important study of 42.8 MeV α-induced fission of Ref. 4 is included in this analysis. The resulting values of $\mathcal{J}_0/\mathcal{J}_{\rm eff}$ are plotted in Fig. 9 as a function of the spin dependent fissility parameter, x_I. This parameter is defined as the fissility x of a nonrotating system with an identical value of $\mathcal{J}_0/\mathcal{J}_{\rm eff}$ as the rotating system. Thus

$$\frac{\mathcal{J}_0}{\mathcal{J}_{\rm eff}}(x_I, I=0)=\frac{\mathcal{J}_0}{\mathcal{J}_{\rm eff}}(x,\langle I^2\rangle)\ , \tag{8}$$

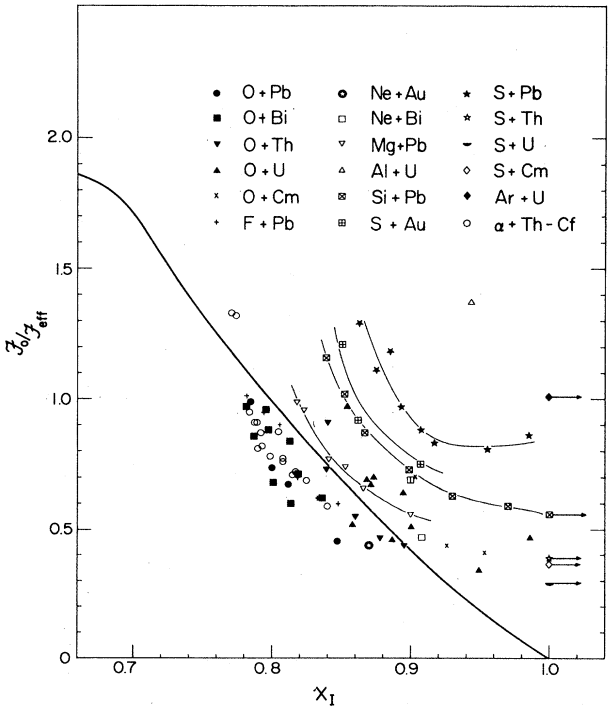

FIG. 9. Experimental $\mathcal{J}_0/\mathcal{J}_{\rm eff}$ values are plotted as a function of the angular momentum corrected fissility x_I (see the text). The solid curve represents the liquid drop model estimate of the saddle point shapes. Open circles represent data for α-induced reactions (Ref. 4).

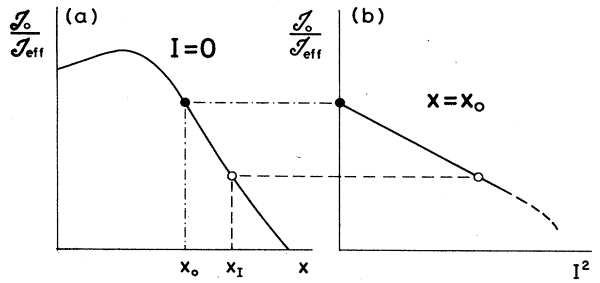

FIG. 10. Schematic illustration of the relation between the fissility, x, of a nonrotating system and the spin-dependent fissility, x_I, of a rotating system.

see Fig. 10.

In Fig. 9 we first note that the $\mathcal{J}_0/\mathcal{J}_{\rm eff}$ values corresponding to the 42.8 MeV α induced reactions (open circles) are systematically smaller than the standard liquid drop model estimate represented by the solid curve. This discrepancy probably arises from the sharp surface approximation of the liquid drop model.[5] More realistic calculations, which incorporate the effects of the finite-range nuclear forces[32] are expected to remove most of this discrepancy. Furthermore, we notice that the $^{16}O+^{208}Pb$, ^{209}Bi, ^{232}Th, and $^{19}F+^{208}Pb$ results are in good agreement with the α-induced data. The reactions of $^{16}O+^{238}U$, $^{20}Ne+^{197}Au$, ^{209}Bi, and $^{24}Mg+^{208}Pb$ are in fair agreement with the liquid drop predictions, whereas there is a clear tendency for higher experimental $\mathcal{J}_0/\mathcal{J}_{\rm eff}$ values for heavier projectiles.

V. CROSS SECTIONS

Based on abundant evidence obtained in recent years, it now appears that heavy ion reactions performed at moderate energies can be classified into four main categories, namely (1) quasielastic reactions, including elastic and inelastic scattering and transfer reactions, (2) deeply inelastic scattering, (3) quasifission, and (4) compound nucleus formation. Each category has special characteristics with respect to energy loss, mass drift, and shape relaxation, and they are generally associated with different angular momenta, reaction times, and regions of occurrence. Thus, the quasielastic reactions are associated with moderate energy losses, and they are generally associated with large impact parameters for which the matter densities of the two ions overlap only slightly and for which the radial kinetic energy is insufficient to surmount the one-dimensional interaction barrier. For center of mass energies above the s-wave interaction barrier, quasielastic reactions are therefore associated with the largest l waves in the reaction.

The characteristic feature of deep inelastic reactions is the larger energy losses associated with this reaction channel. These large energy losses are achieved with small net transfer of mass between the interaction partners. This reaction channel is therefore said to be associated with the strong energy loss mode of heavy ion reactions. Large amounts of mass transfer are observed only for completely relaxed events for which total kinetic energies characteristic of fission fragments are observed.[19] Because of

the complete kinetic energy relaxation such reactions are often labeled quasifission. The associated angular and mass distributions depend critically on the relations between the reaction time, the rotational period, and the rate of mass transfer, respectively. Depending on these relations, quasifission reactions[18,19] bear characteristics of both deeply inelastic scattering and compound nucleus fission. It is the quasifission reactions approaching the latter extreme that have characteristics in terms of mass and angle distribution resembling those of fission following compound nucleus formation. Conceptually we associate the quasifission channel with reactions which fail to form a compound nucleus, and only a quantitative analysis of the mass and angle distributions can differentiate between the two types of reactions as shown in Sec. IV. In fact, quantitative studies of fission mass distributions[33,34] and cross sections[35] provided the first clues of the quasifission process.

In the present study, we are concerned only with data which qualitatively have the characteristics of compound nucleus fission. The analysis of the angular distributions presented in Sec. IV, shows that only some of the reactions studied possess the true characteristics of compound nucleus fission, i.e., that the experimental K_0 values reflect the expected saddle point shapes. The observed deviations from compound nucleus fission depend on the projectile mass and not on the properties of the fused system. We therefore hypothesize that the deviations arise from a contribution of quasifission reactions at large partial waves.

Presently, we will not attempt to estimate the relative contributions from quasifission and compound nucleus fission to the total cross section for symmetric products. This will be the subject of a separate publication.[36] Instead we compare the experimental fission cross sections to the cross sections for overcoming the interaction barrier (the touching cross section) as estimated in the following subsection.

The proximity prescription is used in conjunction with a Coulomb potential for estimating the attractive nuclear potential in order to compute the height of the s-wave interaction barrier. The total ion-ion potential can be written as:

$$V(l,r)=\frac{e^2Z_1Z_2}{r}+\frac{l(l+1)\hbar^2}{2\mu r^2}+V_N(r)\ ; \tag{9}$$

where

$$V_N(r)=4\pi\gamma\bar{c}b\Phi_{\text{prox}}[(r-c_1-c_2)/b]\ ,$$

$$c_i=R_i-b^2/r_i;\ \ \bar{c}=c_1c_2/(c_1+c_2)\ ,$$

$$R_i=1.28A_i^{1/3}-0.76+0.8A_i^{-1/3}\ .$$

Here γ is the surface energy coefficient, b is the diffuseness of the nuclear surface estimated at $b=1$ fm, r is the distance between the centers of the interacting nuclei, and $\Phi_{\text{prox}}(r)$ is the proximity function tabulated by Blocki *et al.*[37] The generalization of the potential to describe interactions between a spherical projectile and a deformed target nucleus is described in detail in Appendix B.

It has been pointed out[18,38] that the standard proximity potential predicts interaction barriers which are, on the average, too large by 2—4%. A substantial fraction of this discrepancy is removed,[19] however, by using a larger value of γ than the one obtained in the liquid drop model.[5] The original value[5] of γ was obtained by using an unrealistically large radius parameter of $r_0=1.2249$ fm. A more recent fit to known nuclear masses and fission barriers performed by Möller and Nix[39] based on a folded Yukawa potential uses a more realistic radius parameter of $r_0=1.16$ fm. As a consequence a larger value of γ is obtained, namely

$$\gamma=1.2496\left[1-2.3\left[\frac{N-Z}{A}\right]^2\right]\ , \tag{10}$$

where N, Z, and A refer to the combined system. This estimate of the surface energy coefficient results in a 20—30% increase in the strength of the nuclear potential as compared to the standard proximity estimate. This gives a 2—3% decrease in the interaction barrier heights improving the agreement with experimental data.

Touching cross sections, calculated on the basis of this modified proximity potential and including the effects of barrier fluctuations caused by shape oscillations as described in Appendix B, are represented by solid curves in Fig. 11.

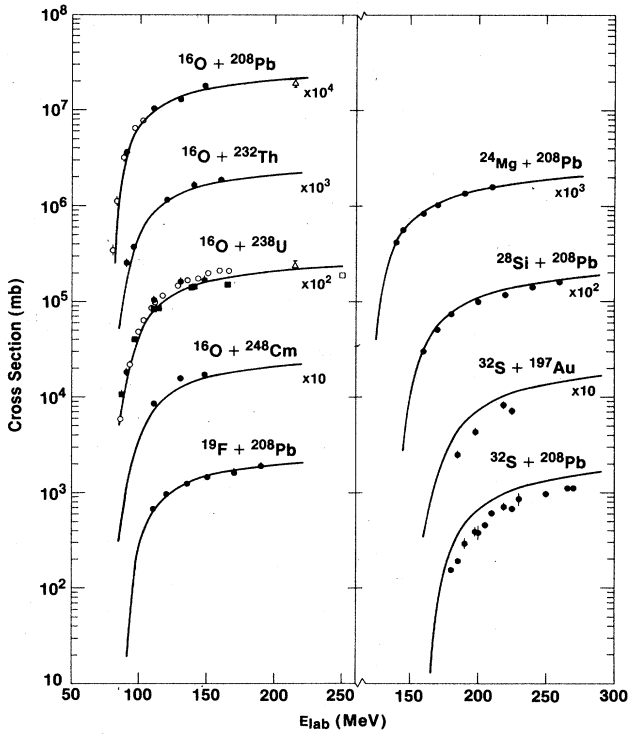

FIG. 11. Comparison of experimental cross sections with theoretical model calculations. Filled circles represent fission cross sections from the present experiment, open circles are taken from Ref. 40 ($^{16}O+^{208}Pb$) and Ref. 41 ($^{16}O+^{238}U$), open triangles are from Ref. 9, and filled squares represent measurements in which full momentum was required (Refs. 12, 16, and 47). The calculated cross sections for touching (solid curves) are shown.

We find that the present prescription for the interaction barrier gives a satisfactory agreement with the measured cross sections for the ^{16}O, ^{19}F, ^{24}Mg, and ^{28}Si induced reactions in the barrier region. It should be kept in mind that the excess cross section seen for $^{16}O+^{238}U$, ^{248}Cm may be caused by contaminations from sequential fission after quasielastic or deeply inelastic reactions. The parameters describing the surface fluctuations of the target nuclei are varied in order to reproduce the slope of the excitation functions at near-barrier energies. The results of this procedure are listed in Table III. We find, that the static deformation of ^{238}U needed to reproduce the excitation function is about 20% lower than the experimentally known value. This discrepancy is most likely associated with the oversimplification of the present model, but we feel that the calculated l distributions are largely insensitive to these deficiencies as long as the sub-barrier cross section is reproduced correctly.

For the ^{32}S-induced reactions we find that the calculated touching cross sections are substantially larger than the experimental fission cross sections. The missing cross section may be associated with deep inelastic scattering, which is not included in the present measurement of the symmetric mass component.

VI. SUMMARY

It has been known for many years that fission angular distributions are dependent on the characteristics of the quantum states available at the fission saddle point.[1] At high excitation energies, where statistical considerations are valid, it has been shown[2] that the angular distributions carry information about the shape of the nucleus at the saddle point via the distribution of K values. Such considerations have proven to be valid for a number of complete fusion reactions which were studied experimentally.[3,4] The comparison of the extracted values of $\mathcal{I}_0/\mathcal{I}_{\text{eff}}$ with the theoretical[5] predictions of the saddle shapes has provided substantial support for the standard theory for fission angular distributions and, in particular, the conservation of the K value selected at the saddle point during the descent to scission.

TABLE III. Parameters used in cross section calculation.

Reaction	V_{touch}[a] (MeV)	$V_{\text{touch}}^{\text{LDM}}$[b] (MeV)	δ_2	σ_2[c]	σ_3[c]
$^{16}O+^{208}Pb$	77.3	78.7			0.03
$^{16}O+^{232}Th$	83.2	84.7	0.19	0.007	
$^{16}O+^{238}U$	84.7	86.1	0.22	0.007	
$^{16}O+^{248}Cm$	87.7	89.2	0.24	0.007	
$^{19}F+^{208}Pb$	85.8	87.3			0.03
$^{24}Mg+^{208}Pb$	113.1	115.1			0.03
$^{28}Si+^{208}Pb$	130.5	132.9			0.03
$^{32}S+^{197}Au$	143.7	146.3			0.05
$^{32}S+^{208}Pb$	147.7	150.4			0.03

[a]Interaction barrier calculated using the surface tension coefficient γ of Eq. (10).
[b]Interaction barrier calculated using liquid drop model (LDM) estimate of surface tension coefficient γ.
[c]See Eq. (B6) for definition.

Recent experimental studies[6–11] of fission angular distributions in heavy ion reactions show distinct deviations from the standard theory, and this has initiated a critical reassessment of its basic assumptions. Several possible deficiencies have been identified in recent years. They fall into three categories: (1) the assumption of fusion (and the formation of a truly equilibrated compound nucleus) during the first step of the reaction is not valid, (2) the distribution of K values is altered during the motion from saddle to scission under influence of the large angular momenta available in heavy ion reactions, and (3) the theoretical prediction of the K distribution at the saddle point is inaccurate because of angular momentum effects unaccounted for by the theories. In the present paper we have assessed each of these possibilities by comparing reactions leading to systems of similar fissility parameter. We conclude that the first of these three assumptions can account for the observed deviations from the standard theory. Fission cross sections for reactions with ^{24}Mg and heavier projectiles appear to have major contributions from quasifission reactions[42,43] in which the observed mass and energy equilibration between the two reaction partners is achieved while the composite system is in close contact, but remains outside the fission saddle point.

ACKNOWLEDGMENTS

We wish to acknowledge Dr. Sven Bjørnholm and Dr. W. J. Swiatecki for many stimulating and illuminating discussions concerning the interpretation of the present data. The tireless support of the Tandem Linac operating staff is greatly appreciated. One of us (B.B.B.) wishes to acknowledge the Danish Natural Science Research Council for partial financial support. This work was performed under the auspices of the Office of High Energy and Nuclear Physics, Division of Nuclear Physics, U.S. Department of Energy, under Contract Number W-31-109-ENG-38.

APPENDIX A: NUMERICAL CALCULATIONS OF $\mathscr{D}$ FUNCTION

The symmetric top wave functions are denoted $\mathscr{D}^I_{MK}(\phi,\theta,\psi)$, where ϕ,θ,ψ are the Euler angles describing the intrinsic body-fixed coordinate system relative to the space-fixed coordinate system, and I, M, and K represent the total spin, and its projection onto a space-fixed and an intrinsic axis, respectively. The $\mathscr{D}$ function can be factorized in the following way:

$$D^I_{MK}(\phi,\theta,\psi)=e^{iM\phi}d^I_{MK}(\theta)e^{iK\psi}\ .$$

Since only the absolute values of the $\mathscr{D}$ functions are needed in the present application, the dependence on the angles ϕ and ψ disappears, and we need only to compute the dependence on the angle θ. In heavy ion reactions involving spin-zero target and projectiles, only $M=0$ states are populated in the composite system, and we can therefore write the appropriate d function[44]

$$d^I_{0K}(\theta)=I!\sqrt{(I-K)!(I+K)!}\sum_{x=K}^{I}(-)^x\frac{(\sin\frac{1}{2}\theta)^{2x-K}(\cos\frac{1}{2}\theta)^{2I+K-2x}}{(I-x)!(I+K-x)!(x-K)!x!}\ . \tag{A1}$$

A particularly simple expression results for the aligned configuration $K=I$, namely

$$d^I_{0I}(\theta)=\frac{\sqrt{(2I)!}}{I!}\left[-\frac{\sin\theta}{2}\right]^I , \tag{A2}$$

which can be computed directly.

In order to compute the d functions for other values of K we make use of the relation between d functions with $M=0$ and the associated Legendre polynomials

$$d^I_{0K}(\theta)=\left[\frac{(I-K)!}{(I+K)!}\right]^{1/2}P^K_I(\theta) \tag{A3}$$

and their recursion relation:[45]

$$P^K_{I+1}(\theta)=[(2I+1)\cos\theta P^K_I(\theta) -(I+K)P^K_{I-1}(\theta)]/(I-K+1)\ . \tag{A4}$$

The corresponding relation for d functions is

$$d^{I+1}_{0K}(\theta)=\frac{1}{\sqrt{(I+1+K)(I+1-K)}} \times[(2I+1)\cos\theta d^I_{0K}(\theta)-\sqrt{(I-K)(I+K)} \times d^{I-1}_{0K}(\theta)]\ . \tag{A5}$$

In the special case of $K=I$ this reduces to

$$d^{I+1}_{0I}(\theta)=\sqrt{2I+1}\cos\theta d^I_{0I}(\theta)\ . \tag{A6}$$

We have used the recursion formulas (A6) and (A5) in conjunction with Eq. (A2) to compute the d function for angles of $\theta=0,1,2,3,4,5,10,15,\ldots,90$ in the range of $I=0$–150 and $K=0$–I and stored the results in a large array with entries for subsequent reference in actual calculations. This method ensures both fast and exact calculations of fission fragment angular distributions.

A classical approximation to fission fragment angular distributions which is frequently used in the literature[46] involves a computation of the following expression:

$$W(\theta)\propto\sum_{I=0}^{\infty}\frac{(2I+1)^2T_I\exp[-(I+\frac{1}{2})^2\sin^2\theta/4K_0^2]J_0[i(I+\frac{1}{2})^2\sin^2\theta/4K_0^2]}{\mathrm{erf}[(I+\frac{1}{2})/(2K_0^2)^{1/2}]}\ , \tag{A7}$$

where J_0 is the zeroth-order Bessel function, and erf is the error function.

In order to evaluate the validity of this classical approximation we have calculated fission fragment anisotropies with both the exact expression Eq. (5) and the classical approximation Eq. (A7) using a triangular spin distribution with maximum spin $I_{\max}$. The results are shown in Fig. 12 as a function of the parameter $p=I^2_{\max}/4K_0^2$, where K_0 is the standard deviation of the Gaussian K distribution Eq. (3).

It is observed that the anisotropy is underestimated by the classical approximation by up to 10%, depending on the angular momentum input.

In our analysis, we have used the exact quantum mechanical expression for the $\mathscr{D}$ functions.

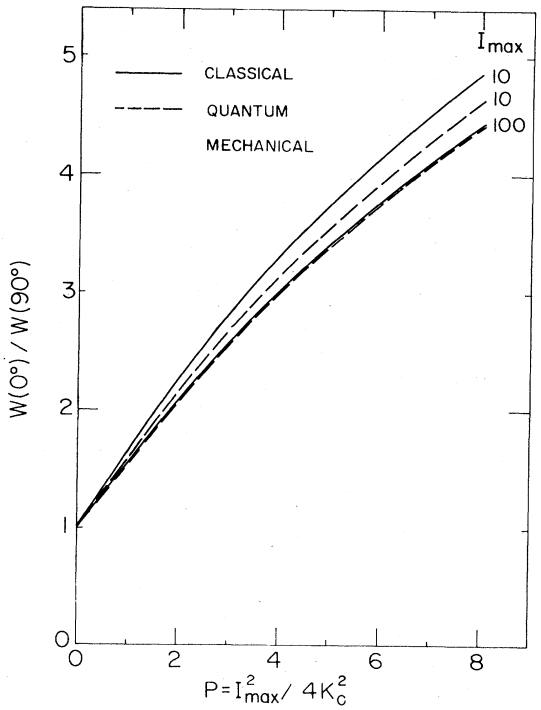

FIG. 12. Calculated fission fragment anisotropies $W(0°)/W(90°)$ are shown as a function of the parameter $p=I^2_{\max}/4K_0^2$. Classical and quantum mechanical calculations are compared for different $I_{\max}$ values.

APPENDIX B: SPIN DISTRIBUTIONS: TARGET DEFORMATION AND SURFACE VIBRATIONS

Several authors have previously studied the effects of static deformations[23–25,47] and surface vibrations[26,27] of the target nucleus on near- and sub-barrier cross sections. In most cases, quite adequate descriptions of the available experimental data may be obtained although anomalies exist[48] which may be due to prefusion nucleon transfer.[27] In the present work we utilize spin-dependent fusion probabilities which result from such model calculations. The parameters of the models are adjusted to reproduce the

measured fission cross sections, a procedure which is believed to result in a more realistic distribution of the partial wave function probabilities.

For the case of an axially symmetric quadrupole deformation we have

$$R(\theta)=C_2[1+\beta Y_{20}(\theta)] . \tag{B1}$$

The interaction potential between target and projectile can be written[49] as

$$V_l(r,\theta,\beta)=\frac{Z_1Z_2e^2}{r}\left[1+\frac{3}{5}\frac{C_2^2}{r^2}\beta Y_{20}(\theta)\right]+\frac{l^2\hbar^2}{2\mu r^2} -4\pi\gamma\frac{C_1C_2}{C_1+C_2}\left[1-2\frac{C_1}{C_1+C_2}\beta Y_{20}(\theta)\right]\Phi_{\text{prox}}[r-C_1-C_2-C_2\beta Y_{20}(\theta)] , \tag{B2}$$

where r is the distance between the centers of the two ions, C_1 and C_2 are the central radii of projectile and target, respectively, γ is the surface energy coefficient, and Φ_{prox} is the proximity function. In this potential we have included a monopole and quadrupole Coulomb term, a centrifugal term, and a nuclear term represented by the proximity potential.[37] (In slight disagreement with Bass,[49] we find a factor of 2 for the deformation dependence of the mean radius curvature for the proximity energy, whereas Bass finds $\frac{5}{2}$.) From Eq. (B2) we observe that the potential does not depend explicitly on both θ and β, but only on the radius deviation $\Delta C=\beta C_2 Y_{20}(\theta)$. Similarly, for octupole deformations, which are relevant for the Pb target, we find an interaction potential,

$$V_l(r,\Delta C)=\frac{Z_1Z_2e^2}{r}\left[1+\frac{3}{7}\frac{C^2\Delta C}{r^3}\right]+\frac{l^2h^2}{2\mu r^2} -4\pi\gamma\frac{C_1C_2}{C_1+C_2}\Phi_{\text{prox}}(r-C_1-C_2-\Delta C) . \tag{B3}$$

For each value of l and $C=C_2+\Delta C$ we can thus find the fusion barrier corresponding to the maximum of the potential given by Eqs. (B2) or (B3). We assume that fusion takes place if the center-of-mass energy exceeds the barrier. The problem of calculating the fusion probability for a specific l value is then reduced to finding the minimum value $C_{\min}$ which leads to fusion and equating the fusion probability with the probability for finding C values larger than $C_{\min}$ for which the fusion barrier is lower. Thus

$$T_l=\int_{C_{\min}}^{\infty}\rho(C)dC , \tag{B4}$$

where T_l is the l-dependent fusion probability and $\rho(C)$ is the probability distribution of the radius.

For zero-point vibrations around a spherical equilibrium the radius deviation follows a Gaussian distribution of the form,

$$\rho(C)=(2\pi\sigma_\lambda^2)^{-1/2}\exp[-(C-C_2)^2/2\sigma_\lambda^2] , \tag{B5}$$

where the standard deviation is given by the relation,

$$\sigma_\lambda=\frac{C_2}{Z(\lambda+3)}\left[(2\lambda+1)\frac{B(E\lambda)}{B_{\text{s.p.}}(E\lambda)}\right]^{1/2} , \tag{B6}$$

where λ is the multipolarity and $B(E\lambda)/B_{\text{s.p.}}(E\lambda)$ is a measure of the collectivity of the lowest collective states of the target nucleus. In this case, the fusion probability is given by the error function,

$$T_l=\tfrac{1}{2}\{1-\text{erf}[(C-C_2)/\sqrt{2\sigma_\lambda^2}]\} \quad C>C_2 , \qquad =\tfrac{1}{2}\{1+\text{erf}[(C_2-C)/\sqrt{2\sigma_\lambda^2}]\} \quad C<C_2 . \tag{B7}$$

For a statically quadrupole deformed nucleus one finds the distribution

$$\rho_\beta(C)=\left[2C_2\delta^{1/2}\left[\frac{C-C_2}{C_2}+\frac{\delta}{3}\right]^{1/2}\right]^{-1} ; \qquad -\frac{\delta}{3}\le\frac{C-C_2}{C_2}\le\frac{2}{3}\delta , \tag{B8}$$

$$=0; \text{ elsewhere} ,$$

where $\delta=\frac{3}{2}\sqrt{5/4\pi}\beta$.

In the harmonic oscillator approximation the β-vibrational wave function in the ground state is given by

$$\rho(\beta)=\left\{\sqrt{2\pi\sigma_\beta^2}\right\}^{-1}\exp\left[-\frac{(\beta-\beta_0)^2}{2\sigma_\beta^2}\right] , \tag{B9}$$

where the σ_β is given by Eq. (11) in Ref. 26. For a target nucleus which is β vibrating around an equilibrium quadrupole shape described by the deformation β_0, we thus find the following distribution of the radius deviation,

$$\rho(C)=\int_{-\infty}^{\infty}\rho(\beta)\rho_\beta(C)d\beta =(2\pi\sigma^2)^{-1/2}\int_{-\infty}^{\infty}\exp\left[-\frac{(\beta-\beta_0)^2}{2\sigma_B^2}\right]\rho_\beta(C)d\beta . \tag{B10}$$

This integral can easily be solved numerically using Gaussian quadrature.

Distributions of radius deviations for surface vibrating spherical and statically deformed targets are compared in Fig. 13 as well as their integrals, which correspond to the fusion probability. It should be noted that the two distributions have the same variance. The effect of the choice of l distribution on the values of $\mathcal{J}_0/\mathcal{J}_{\text{eff}}$ extracted from the fit to the fission angular distributions is illustrated in Fig. 14 for the $^{16}O+^{232}Th$ system. This comparison shows that the use of spin distributions, with tails consistent with the near-barrier cross section, results in

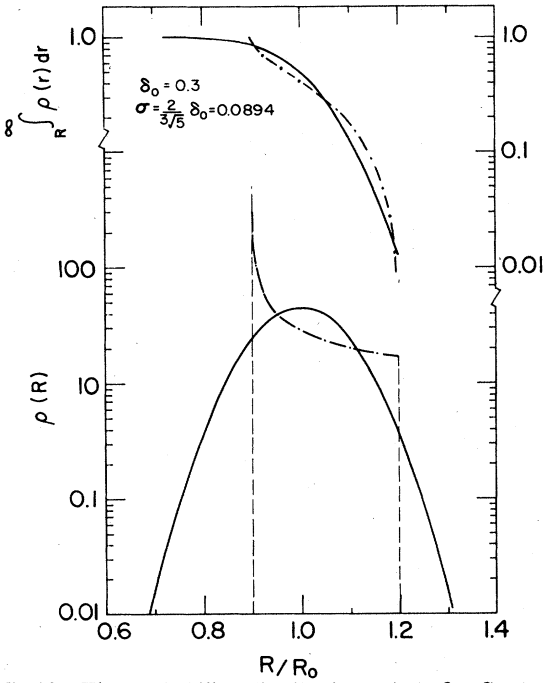

FIG. 13. The probability distribution, $\rho(R)$, for finding the nuclear surface at a distance R is plotted as a function of the reduced radius R/R_0 for deformed (dashed-dotted curve) and a spherical vibrating (solid curve) nucleus. The integrals of the distribution are shown in the upper section of the figure.

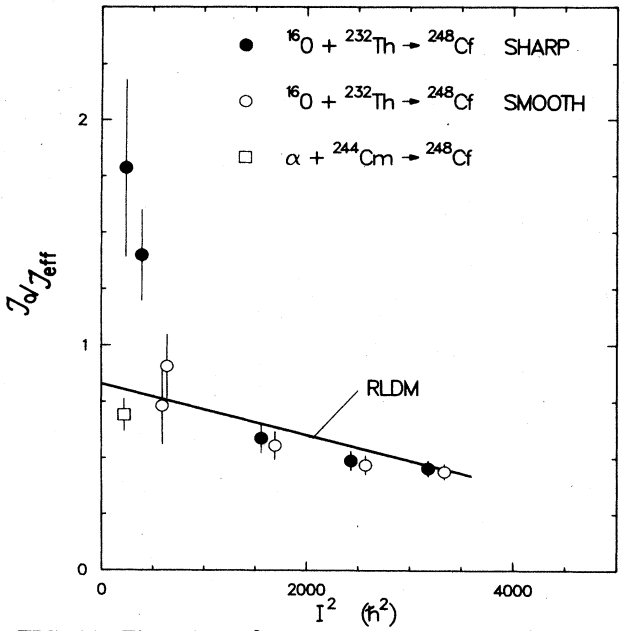

FIG. 14. The values of $\mathcal{J}_0/\mathcal{J}_{\text{eff}}$ are shown as a function of the mean squared spin $\langle I^2 \rangle$ for sharp cutoff (solid points) and smooth (open circles) l distributions, for the $^{16}O+^{232}Th$ reaction. The $\mathcal{J}_0/\mathcal{J}_{\text{eff}}$ for the $\alpha+^{244}Cm$ reaction (open square) and the rotating liquid drop model estimate (solid curve) are shown for comparison.

$\mathcal{J}_0/\mathcal{J}_{\text{eff}}$ values, which agree well with the RLDM estimate. In cases where the saddle point shape is known from measurements with lighter projectiles, this effect actually provides a sensitive measure of the near-barrier spin distribution in heavy-ion-fusion reactions.

APPENDIX C: POST-SCISSION REORIENTATION

In the absence of rapid rotations it is normally assumed that the fission fragments after scission will follow linear trajectories given by the orientation of the scission configuration. If, however, the system possesses a large collective angular momentum as scission, the fragments are expected to follow hyperbolic trajectories in the plane perpendicular to the collective spin vector $R=\sqrt{I(I+1)-K^2}$, describing the collective rotation of the system, see Fig. 15. The classical Coulomb trajectories are described by the equation,

$$r=\frac{l^2}{\mu Z_1 Z_2 e^2}\frac{1}{\epsilon\cos\phi-1}\,, \tag{C1}$$

where r is the distance between the fragment centers, μ is the reduced mass, l is the orbital angular momentum, and ϕ is the angle through which the system has rotated since scission. The eccentricity ϵ can be evaluated at the scission point corresponding to $\phi=0$,

$$\epsilon=\frac{l^2 r_{sc}}{\mu r_{sc}^2 Z_1 Z_2 e^2}+1=\frac{2E_R+E_C}{E_C}\,, \tag{C2}$$

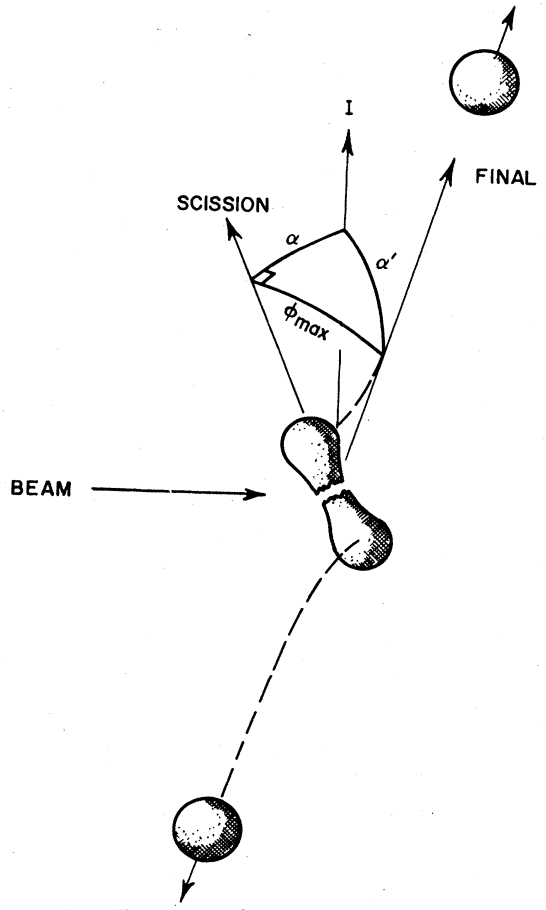

FIG. 15. Illustration of post-scission trajectories.

where E_R and E_C are the energies in orbital motion and Coulomb repulsion at the scission point, respectively. The angle $\phi_{\max}$ between the symmetry axis at scission and the asymptotic direction of the fission fragments is found from Eq. (C1),

$$\cos\phi_{\max}=\frac{1}{\epsilon}=\frac{E_C}{2E_R+E_C} . \tag{C3}$$

The angle α' between the direction of the fully accelerated fragments and the spin axis can now be computed by considering the spherical triangle expanded by the spin vector, the symmetric axis at scission, and the direction of final fragments, see Fig. 15. Using the spherical cosine relation we find

$$\cos\alpha'=\cos\phi_{\max}\cos\alpha , \tag{C4}$$

where the angle α is given by the K value at scission

$$\cos\alpha=K/I . \tag{C5}$$

Denoting the total final helicity K', i.e., $\cos\alpha'=K'/I$ we find

$$K'=K\frac{E_C}{2E_R+E_C} . \tag{C6}$$

This relation describes the change in total helicity during reseparation brought about by orbital motion in the exit channel.

In general, we expect that the energy in relative rotation at scission E_R depends on the K value. Assuming that the sticking condition is fulfilled at scission, the orbital angular momentum l is a fraction f of the total collective angular momentum, namely,

$$l=f\cdot R=f\sqrt{I(I+1)-K^2} . \tag{C7}$$

The rotational energy at scission is then given by

$$E_R=f^2\frac{I(I+1)-K^2}{2\mathcal{J}_{12}} , \tag{C8}$$

where $\mathcal{J}_{12}$ is the relative nonaxial moment of inertia at scission. By insertion into Eq. (B6) and solving for K, we find

$$K=[\sqrt{1+4a(1+b)K'^2}-1]/2aK' , \tag{C9}$$

where $a=f^2/E_C\mathcal{J}_{12}$ and $b=aI(I+1)$. The final K distribution is given now by

$$\rho(K')=\frac{dK}{dK'}\rho(K)=\frac{1-[1+4a(1+b)K'^2]^{-1/2}}{\sqrt{8\pi}aK_0K'^2}\times\exp\left\{-\frac{1}{2}\left[\frac{\sqrt{1+4a(1+b)K'^2}-1}{2aK'K_0}\right]^2\right\} . \tag{C10}$$

Although this expression is somewhat complicated, it reduces to a normal Gaussian distribution if the rotational energy is small relative to the Coulomb repulsion at scission, i.e., $4a(1+b)K'^2\ll 1$.

In this limit we find

$$\rho(K')=\frac{1}{\sqrt{2\pi}K_0'}\exp\left[-\frac{1}{2}\left[\frac{K'}{K_0'}\right]^2\right] , \tag{C11}$$

where

$$K_0'=K_0\frac{E_C}{2E_R+E_C} . \tag{C12}$$

To first order one can account for the effects of centrifugal forces at scission on the fission angular distributions by multiplying the K_0 value expected at the scission point by a correction factor which depends on the ratio of Coulomb to centrifugal energies at scission.

A crude estimate of this effect can be obtained by approximating the scission configuration by two touching equal size spheres in rigid rotation. In this case we find

$$\frac{2E_R}{E_C}\simeq 122\frac{I^2}{A^{4/3}Z^2} . \tag{C13}$$

A recent study of the angular momentum dependence of the total kinetic energy release in S+Sm reactions[47] indicates that this ratio of centrifugal to Coulomb energies at the scission point is approximately correct although each quantity may be somewhat overestimated by this simplified model of the scission point shape. We have therefore used this expression to estimate the associated correction to the extracted values of K_0^2. Thus we find

$$K_0^2=(K_0')^2\left[1+122\frac{I^2}{A^{4/3}Z^2}\right]^2 \tag{C14}$$

or, expressed in terms of the fissility parameter x and the y parameter of the rotating liquid drop model,[17] we find

$$K_0^2=(K_0')^2(1+1.245y/x)^2 , \tag{C15}$$

where K_0' is the standard deviation of the final (measured) total helicity distribution and K_0 is the standard deviation of the K distribution at scission, which normally is assumed identical to the saddle point K distribution. Applying this correction to the extracted value of the $\mathcal{J}_0/\mathcal{J}_{\rm eff}$ parameter we find

$$\frac{\mathcal{J}_0}{\mathcal{J}_{\rm eff}^{\rm sc}}\simeq\left.\frac{\mathcal{J}_0}{\mathcal{J}_{\rm eff}}\right|_{\rm meas}(1+1.245y/x)^{-2} . \tag{C16}$$

Having chosen to express this correction in terms of the parameters x and y we can show universal contours of the correction term in the x-y plane as illustrated in Fig. 16.

APPENDIX D: SEQUENTIAL FISSION CONTRIBUTION

The measurement of fission fragments in the present work did not include a determination of the momentum transfer, and we therefore cannot discriminate against fission following transfer reactions and/or inelastic excitations of the target nucleus. The contamination of the present data from such reactions can be significant in cases of fissionable target nuclei. It is therefore important to estimate the magnitude of sequential fission in such cases in order to judge its effect on the extracted values of $\mathcal{J}_0/\mathcal{J}_{\rm eff}$.

In the case of $^{16}O+^{238}U$, information on the sequential fission contribution has been obtained from measurements of the folding angle between the two fission frag-

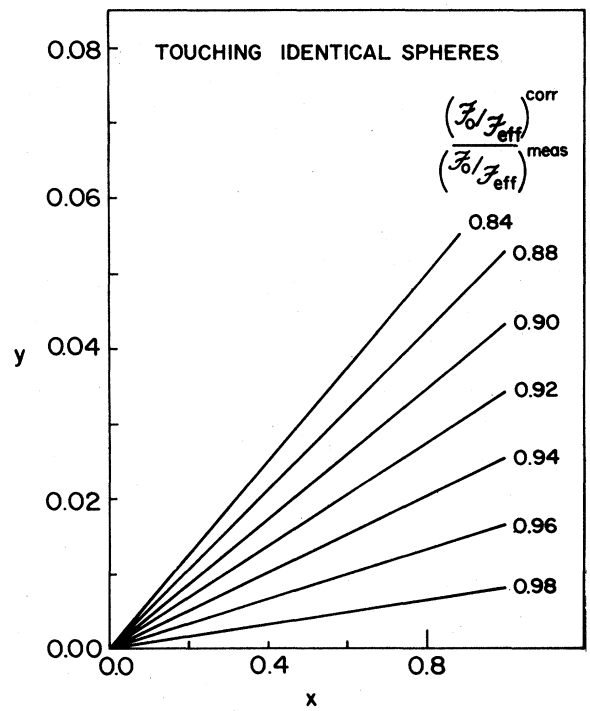

FIG. 16. Contours of the correction factor due to post scission reorientation are shown in an x-y diagram.

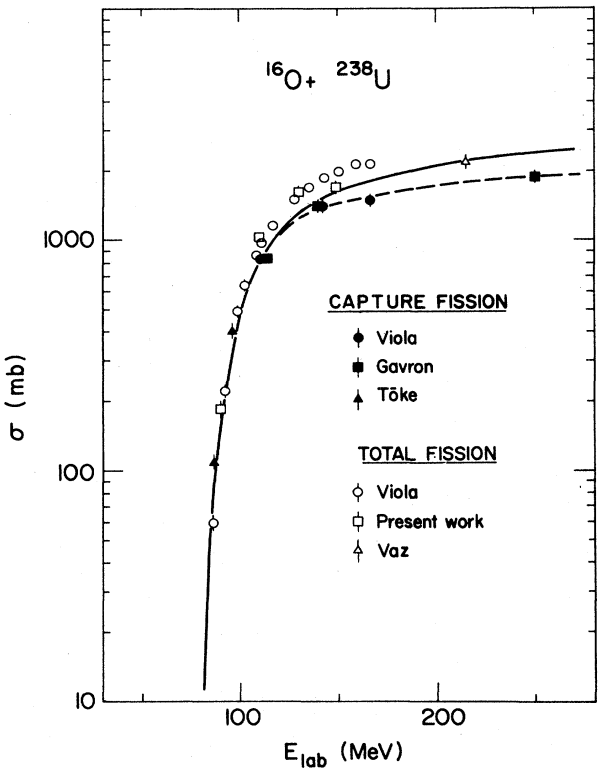

FIG. 17. Excitation functions for fission following full momentum transfer reactions (solid points) and total fission (open points) are compared to the cross section for touching (solid curve). The dashed curve represents the experimental estimate of the fission cross section for full momentum reactions obtained by a smooth interpolation between experimental points.

ments,[50–52] which have recently been analyzed by Viola *et al.*[53] The known fission cross sections for the $^{16}O+^{238}U$ systems are presented in Fig. 17. Measurements of the total fission cross sections (which include sequential fission) are represented by open symbols, whereas measurements, which exclude the sequential fission component, are shown as solid symbols. It should be noted that the estimate of the sequential fission contribution from the folding angle distribution[51] measured at $\theta_{c.m.}=90°$ is based on the assumption that the anisotropy of this fraction is identical to the anisotropy of the total cross section.

The solid curve in Fig. 17 represents the calculated touching cross section (see Sec. V), which is smaller than the total measured fission cross section (open symbols). The excess measured cross section is believed to stem from sequential fission following quasielastic reactions. This component is even more pronounced in the case of $^{16}O+^{248}Cm$, but significantly smaller for $^{16}O+^{232}Th$, as expected due to the dependence on target fissility (see Fig. 11). The difference between the calculated touching cross section (solid) curve and the measured capture fission cross section (solid symbols and dashed curve) is believed to be due to sequential fission following deep inelastic reactions.

In order to estimate the uncertainty in the analysis caused by the sequential fission contribution we have performed the correction under two extreme assumptions about the anisotropy of the sequential fission contribution. We first assume that the anisotropy is the same as for the compound fission part. In this case the analysis can be

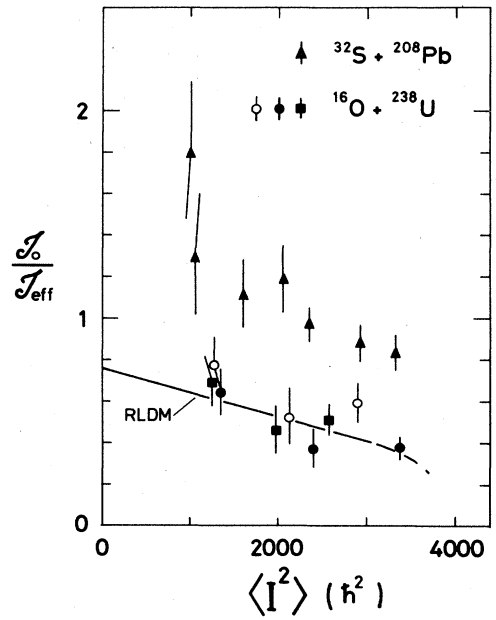

FIG. 18. Illustration of the possible effects of sequential fission reactions on the angular anisotropies for $^{16}O+^{238}U$. $\mathcal{I}_0/\mathcal{I}_{eff}$ values obtained without correcting for sequential fission are represented by solid circles. The solid squares are corrected for sequential fission assuming that the anisotropy for this component is identical to the measured one. For the open circles an isotropic angular distribution was assumed.

performed by using the compound fission cross section in the estimate of the spin distribution of the fissioning system. Values of $\mathcal{J}_0/\mathcal{J}_{\text{eff}}$ obtained this way are plotted in Fig. 18 as solid squares and compared to the uncorrected values (filled circles). We observe that this method of correction results in slightly larger values of $\mathcal{J}_0/\mathcal{J}_{\text{eff}}$, which however, correspond to somewhat smaller values of the mean square spin $\langle I^2 \rangle$ due to the reduction of the cross section estimate.

In the other extreme we assume that the sequential contribution is isotropically distributed. Since the relative sequential fission contribution is measured at $\theta_{\text{c.m.}} \sim 90°$ by the folding angle method, this assumption leads to a slightly smaller estimate of the total sequential fission contribution. When the data are corrected for this contribution, we find an increased anisotropy for the compound fission part which is reflected in the larger values of $\mathcal{J}_0/\mathcal{J}_{\text{eff}}$ as shown by the open circles. However, the difference in $\mathcal{J}_0/\mathcal{J}_{\text{eff}}$ values obtained under the two extreme assumptions is quite small and the discrepancy between the $^{16}O+^{238}U$ and the $^{32}S+^{208}Pb$ reactions persists. We therefore feel justified in concluding that this observed discrepancy is an effect of entrance channel conditions (mass asymmetry), and that it cannot trivially be accounted for by the sequential fission contribution. In the analysis of reactions on fissionable targets presented in the main text we have corrected for sequential fission under the assumption of equal anisotropy for the two components.

In the case of $^{16}O+^{232}Th$, we expect a much smaller contribution of sequential fission due to the smaller fissility of nuclei in the Th region as compared to the U region. We have therefore used calculated capture cross sections in the analysis of the angular distributions, which results in only minor corrections when compared to the results obtained with the measured fission cross sections.

We have also performed a similar correction to the $^{16}O+^{248}Cm$ data. In this case, the $\mathcal{J}_0/\mathcal{J}_{\text{eff}}$ values move even further away from the rotating liquid drop model estimate, and there seems to be a real discrepancy. As mentioned earlier, the fission barrier is very small (< 1 MeV) in this case, and it is not unreasonable to expect that the significance of the saddle point in controlling the angular distributions is lost, although other explanations such as non-K-conservation under the prolonged descent from saddle to scission or the onset of quasifission could be the cause of the large discrepancy in this case.

---

*Present address: Physics Department, University of Pennsylvania, Philadelphia, PA 19104.

†Present address: Nuclear Science Division, Lawrence Berkeley National Laboratory, Berkeley, CA 94720.

[1]Aage Bohr, *Proceedings of the United Nations International Conference on the Peaceful Uses of Atomic Energy, Geneva, Switzerland, 1955* (United Nations, New York, 1956), Vol. 2, p. 151.

[2]I. Halpern and V. M. Strutinsky, *Proceedings of the Second United Nations International Conference on the Peaceful Uses of Atomic Energy, Geneva, Switzerland, 1957* (United Nations, Geneva, Switzerland, 1958), p. 408.

[3]G. L. Bate, R. Chaudhry, and J. R. Huizenga, Phys. Rev. **131**, 722 (1963).

[4]R. F. Reising, G. L. Bate, and J. R. Huizenga, Phys. Rev. **141**, 1161 (1966).

[5]W. D. Myers and W. J. Swiatecki, Ark. Fys. **36**, 343 (1967).

[6]B. B. Back, H.-G. Clerc, R. R. Betts, B. G. Glagola, and B. D. Wilkins, Phys. Rev. Lett. **46**, 1068 (1981).

[7]K. T. Lesko, S. Gil, A. Lazzarini, V. Metag, A. G. Seamster, and R. Vandenbosch, Phys. Rev. C **27**, 2999 (1983).

[8]B. B. Back, R. R. Betts, K. Cassidy, B. G. Glagola, J. E. Gindler, L. E. Glendenin, and B. D. Wilkins, Phys. Rev. Lett. **50**, 818 (1983).

[9]L. C. Vaz, D. Logan, E. Duek, J. M. Alexander, M. F. Rivet, M. S. Zisman, M. Kaplan, and J. W. Ball, Z. Phys. A **315**, 169 (1984).

[10]M. B. Tsang, H. Utsunomiya, C. K. Gelbke, W. G. Lynch, B. B. Back, S. Saini, P. A. Baisden, and M. A. McMahan, Phys. Lett. **B129**, 18 (1983).

[11]M. B. Tsang, D. Ardouin, C. K. Gelbke, W. G. Lynch, Z. R. Xu, B. B. Back, R. R. Betts, S. Saini, P. A. Baisden, and M. A. McMahan, Phys. Rev. C **28**, 747 (1983).

[12]A. Gavron, P. Eskola, A. J. Sierk, J. Boissevain, H. C. Britt, K. Eskola, M. M. Fowler, H. Ohm, and J. B. Wilhelmy, Phys. Rev. Lett. **52**, 589 (1984).

[13]V. E. Viola, Jr., T. D. Thomas, and G. T. Seaborg, Phys. Rev. **129**, 2710 (1963).

[14]S. A. Karamyan, I. V. Kuznetsov, T. A. Muzycka, Yu. Ts. Oganesyan, Yu. E. Penionzkevich, and B. J. Pustyl'nik, Yad. Fiz. **6**, 494 (1967) [Sov. J. Nucl. Phys. **6**, 360 (1968)].

[15]H. Rossner, D. Hilscher, E. Holub, G. Ingold, U. Jahnke, H. Orf, J. R. Huizenga, J. R. Birkelund, W. U. Schröder, and W. W. Wilcke, Phys. Rev. C **27**, 2666 (1983).

[16]J. Tōke, R. Bock, Dai Guang-xi, A. Gobbi, S. Gralla, K. D. Hildenbrand, J. Kuzminski, W. F. J. Müller, A. Olmi, W. Reisdorf, S. Bjørnholm, and B. B. Back, Phys. Lett. **142B**, 258 (1984).

[17]S. Cohen, F. Plasil, and W. J. Swiatecki, Ann. Phys. (N.Y.) **82**, 557 (1974).

[18]R. Bock, Y. T. Chu, M. Dakowski, A. Gobbi, E. Grosse, A. Olmi, H. Sann, D. Schwalm, U. Lynen, W. Müller, S. Bjørnholm, H. Esbensen, W. Wölfli, and E. Morenzoni, Nucl. Phys. **A388**, 334 (1982).

[19]J. Tōke, G. X. Dai, S. Gralla, A. Gobbi, K. D. Hildenbrand, W. F. J. Müller, A. Olmi, H. Stelzer, B. B. Back, and S. Bjørnholm, Nucl. Phys. A (in press).

[20]H. Henschel and R. Schmidt, Nucl. Instrum. Methods **151**, 529 (1978).

[21]V. E. Viola, Jr., Nucl. Data **A1**, 391 (1966).

[22]H. Ho and P. L. Gonthier, Nucl. Instrum. Methods **190**, 75 (1981).

[23]C. Y. Wong, Phys. Rev. Lett. **31**, 766 (1973).

[24]R. G. Stokstad, Y. Eisen, S. Kaplanis, D. Pelte, U. Smilanski, and I. Tserruya, Phys. Rev. Lett. **41**, 465 (1978).

[25]W. Reisdorf, F. P. Hessberger, K. D. Hildenbrand, S. Hofman, G. Münzenberg, K.-H. Schmidt, J. H. R. Schneider, W. F. W. Schneider, S. Sümmerer, G. Wirth, J. V. Kratz, and K. Schlitt, Phys. Rev. Lett. **49**, 1811 (1982).

[26]H. Esbensen, Nucl. Phys. **A352**, 147 (1981).

[27]R. A. Broglia, C. H. Dasso, S. Landowe, and G. Pollarolo, Phys. Lett. **133B**, 34 (1983).

[28]D. v. Harrach, P. Glässel, Y. Civelekoglu, R. Männer, H. J. Specht, J. B. Wilhelmy, H. Freiesleben, and K. D. Hildenbrand, *Proceedings of the International Symposium on Physics and Chemistry of Fission, Jülich, 1979* (IAEA, Vienna, 1980), p. 575.

[29]P. Bond, Phys. Rev. Lett. **52**, 414 (1984); and (unpublished).

[30]H. H. Rossner, J. R. Huizenga, and W. U. Schröder, Phys. Rev. Lett. **53**, 38 (1984).

[31]M. Prakash, V. S. Ramamurthy, S. S. Kapoor, and J. M. Alexander, Phys. Rev. Lett. **52**, 990 (1984).

[32]A. Sierk (unpublished).

[33]C. Lebrun, F. Hanappe, J. F. Lecolley, F. Lefebvres, C. Ngô, J. Peter, and B. Tamain, Nucl. Phys. **A321**, 207 (1979).

[34]B. Borderie, M. Berlanger, D. Gardes, F. Hanappe, L. Nowicki, J. Peter, B. Tamain, S. Agarwall, J. Girard, C. Gregoire, J. Mutuszek, and C. Ngô, Z. Phys. A **299**, 263 (1981).

[35]B. Heusch, C. Volant, H. Freiesleben, R. P. Chestnut, K. D. Hildenbrand, F. Pühlhofer, W. F. W. Schneider, B. Kohlmeyer, and W. Pfeffer, Z. Phys. A **288**, 391 (1978).

[36]B. B. Back, Phys. Rev. C **31**, 2104 (1985).

[37]J. Blocki, J. Randrup, W. J. Swiatecki, and C. F. Tsang, Ann. Phys. (N.Y.) **105**, 427 (1977).

[38]L. C. Vaz, J. M. Alexander, and G. R. Satchler, Phys. Rep. **69**, 373 (1981).

[39]P. Möller and J. R. Nix, At. Data Nucl. Data Tables **26**, 165 (1981).

[40]F. Videbaek, R. B. Goldstein, L. Grodzins, S. G. Steadman, T. A. Belote, and J. D. Garrett, Phys. Rev. C **15**, 954 (1977).

[41]V. E. Viola, Jr. and T. Sikkeland, Phys. Rev. **128**, 767 (1962).

[42]W. J. Swiatecki, Phys. Scr. **24**, 113 (1981).

[43]S. Bjørnholm and W. Swiatecki, Nucl. Phys. **391**, 471 (1982).

[44]A. R. Wigner, *Group Theory and Its Application to the Quantum Mechanics of Atomic Spectra* (Academic, New York, 1959).

[45]A. R. Edmonds, *Angular Momentum in Quantum Mechanics* (Princeton University, Princeton, New Jersey, 1957).

[46]J. R. Huizenga, A. N. Behkami, and L. G. Moretto, Phys. Rev. **177**, 1826 (1969).

[47]B. G. Glagola, B. B. Back, and R. R. Betts, Phys. Rev. C **29**, 486 (1983).

[48]M. Beckerman, M. Salomaa, A. Sperduto, H. Enge, J. Ball, A. DiRienzo, S. Gazes, Yan Chen, J. D. Molitoris, and Mao Nai-feng, Phys. Rev. Lett. **45**, 1472 (1980).

[49]R. Bass, *Nuclear Reactions with Heavy Ions* (Springer, Berlin, 1980), p. 346.

[50]T. Sikkeland, E. L. Haines, and V. E. Viola, Jr., Phys. Rev. **125**, 1350 (1962).

[51]T. Sikkeland and V. E. Viola, Jr., *Proceedings of the 3rd Conference on Reactions between Complex Nuclei* (University of California, Berkeley, 1963), p. 232.

[52]B. B. Back, K. L. Wolf, A. C. Mignerey, C. K. Gelbke, T. C. Awes, H. Breuer, V. E. Viola, Jr., and P. Dyer, Phys. Rev. C **22**, 1927 (1980).

[53]V. E. Viola, Jr., B. B. Back, K. L. Wolf, T. C. Awes, C. K. Gelbke, and H. Breuer, Phys. Rev. C **26**, 178 (1982).